ANOTHER LOOK AT SONIC THERMOMETRY

(Research Note)

J. C. KAIMAL and J. E. GAYNOR
NOAA/ERL/Wave Propagation Laboratory, Boulder, Colorado 80303, U.S.A.

(Received in final form 12 November, 1990)

Abstract. In this note we reassess the role of sonic thermometry in boundary-layer studies. The sonic temperature signal, when corrected for crosswind velocity contamination, very closely approximates the virtual temperature of air. This variable is needed for many boundary-layer calculations. We describe preliminary tests with a new sonic anemometer-thermometer that performs the velocity correction in real time. Our test results offer new insights into the nature of the velocity error on temperature standard deviations and fluxes. They also draw attention to the high noise threshold that appears as an f^{+1} rise in the $fS(f)$ spectrum when spectral levels drop below 10^{-4}°C^2.

Introduction

Ever since Suomi (1957) first attempted to measure surface-layer wind and temperature turbulence with a sonic anemometer-thermometer, the idea of extracting both vertical wind and temperature fluctuations within the same sampling volume from the same set of acoustic measurements has held a special appeal for micrometeorologists. Subsequent versions of the instrument, described by Kaimal and Businger (1963) and Mitsuta (1966, 1974), proved more dependable for field operation, but the technique used to derive temperature had serious flaws that inhibited use of those versions in field experiments for over a decade.

In these early sonic thermometers, the temperature signal was the sum of transit times for sound transmitted in opposite directions across a known path (the transit time difference yielded the velocity component along the path). This term is not linearly related to temperature, is contaminated by the wind components normal to and along the path and by humidity, and has a calibration that is sensitive to temperature. Although a linear approximation could be justified for small deviations in temperature and the humidity error ignored for measurements over land, the velocity contamination proved significant (Kaimal, 1969) in neutral and stable stratifications when temperature fluctuations tend to vanish or become very small.

A breakthrough was achieved in 1979 when Kaijo Denki, Inc., introduced their new sonic anemometer-thermometer (Hanafusa *et al.*, 1982), which computed winds and temperatures from the reciprocals of the transit times. Using digital processing hardware, they were able to provide outputs directly in degrees K, but the sensitivity to horizontal wind and humidity remained. Schotanus *et al.* (1983), in an excellent treatment of the problem, showed how these two effects can be

Boundary-Layer Meteorology **56**: 401–410, 1991.

removed from the temperature statistics if data from concurrent measurements of momentum fluxes and humidity flux are available.

In the new Applied Technologies, Inc. (ATI), sonic anemometer-thermometer (Model SWS/3K), the same microprocessor controlling its sonic anemometer functions also performs the calculations required to compute temperature along its vertical path, including the correction for velocity contamination. This leaves only the humidity effect to account for. In the sections to follow, we discuss the underlying theory and some preliminary results of tests conducted on the ATI instrument. The tests were made during an experiment conducted at the Boulder Atmospheric Observatory (BAO) (Kaimal and Gaynor, 1983) to evaluate the flow distortion characteristics of ATI's acoustic probe. Sonic thermometry bears reexamination since it brings with it some distinct advantages: compatibility in spatial and temporal resolution with the vertical wind component; collocation of the two sampling volumes; predictable calibration, unaffected by aging or atmospheric contamination; and, for marine applications, freedom from "cold spikes" (Schmitt *et al.*, 1978) resulting from salt deposition on platinum wire and similar immersion-type sensors.

2. Sonic Temperature Measurement

The strong dependence of sound speed on temperature forms the basis for this method of measuring temperature. The relationship most commonly invoked (Kaimal and Businger, 1963) is

$$c^2 = 403\,T(1 + 0.32e/p)\,, \tag{1}$$

where c is the velocity of sound ($\mathrm{m\,s^{-1}}$) in air, T is the temperature (K), and e and p are, respectively, the vapor pressure of water in air and the absolute pressure. The temperature derived from the speed of sound measurement in air has the same form as the virtual temperature T_v, defined by meteorologists as the temperature at which dry air has the same density as moist air at the same pressure.

$$T_v = T(1 + 0.38e/p)\,, \tag{2a}$$

or, in terms of specific humidity, q,

$$T_v = T(1 + 0.61q)\,, \tag{2b}$$

because $q \simeq 0.622e/p$. At least in one related field, radio acoustic sounding (May *et al.*, 1990), the derived temperature is referred to simply as virtual temperature. Micrometeorologists have, in the past, maintained the distinction,* referring to the acoustically derived temperature as sonic virtual temperaure or, simply, sonic

* The difference arises from the fact that the coefficient of e/p in (2) is $(1 - M_w/M_a)$ where M_w and M_a are the molecular weights for water vapor and air, while that in (3) is $(\gamma_w/\gamma_a - M_w/M_a)$, where γ_w and γ_a are the ratio of specific heats for water vapor and air (Miller, 1937).

temperature. Retaining this disinction for the present and denoting the sonic temperature by T_s, where

$$T_s = T(1 + 0.32e/p)\,, \tag{3}$$

the output of the sonic thermomeer assumes the form

$$T_s = (d^2/1612)(1/t_1 + 1/t_2)^2 + (1/403)\,V_n^2\,, \tag{4}$$

where d (= 0.15 m) is the acoustic path length, oriented vertically, t_1 and t_2 are the transit times in seconds for acoustic pulses traveling in opposite directions across d, and V_n is the magnitude of the horizontal wind vector in meters per second (Appendix A). Here V_n^2 can be replaced by $V_X^2 + V_Y^2$, where V_X and V_Y are the horizontal wind components measured along the probe's X and Y axes, and corrected for transducer shadow error as described by Kaimal *et al.* (1990).

In many boundary-layer calculations, the virtual temperature rather than the true temperature is needed to include the buoyancy contribution from moisture. For example, the virtual temperature flux is the appropriate flux to use when calculating the Monin–Obukhov stability parameter z/L. The same holds for the buoyant production term in the turbulent kinetic energy budget. Over open land, the difference is small and often ignored. But in plant canopies and in the marine boundary layer, where temperature fluctuations are small and the moisture fluctuations large, the differences can be very significant. In such applications and even over moderately moist ground, the closeness of T_s to T_v can be viewed as an advantage. It is instructive, therefore, to examine the errors incurred in assuming $T_s = T$ and $T_s = T_v$.

If T and p can be assumed constant for any observing interval, we can write

$$T_s \approx \begin{cases} T + (0.32\,T/p)e \approx T + 0.1e \\ T_v - (0.06\,T/p)e \approx T_v - 0.02e \end{cases}, \tag{5}$$

where the temperatures and pressures are expressed in K and mb, respectively. The offsets in T and T_v are large, up to +2.4°C in T and −0.48°C in T_v for saturated air at sea level, if the humidity correction is ignored. But the short-term fluctuations in the vapor pressure are usually much smaller than their mean value. For standard deviation $\sigma_e \approx 0.5$ mb, typical at 10 m above very moist ground, the standard deviation of the errors encountered would be around 0.05°C in T and 0.01°C in T_v, the latter being well within the bounds of experimental uncertainty.

3. Testing the Sonic Temperature Output

A definitive test of the sonic temperature measurement would involve concurrent fast-response humidity measurements close to either the sonic temperature path or to the fine-wire platinum thermometer used for comparison. In either case, it raises the spectre of flow distortion errors in the measurements which we do not

yet fully understand. Short of such a test, one can look for the effects of humidity and V_n^2 in the turbulence statistics, the approach we have taken in this preliminary study.

In the lower boundary layer, the temperature and humidity fluctuations are very highly correlated, nearly +1 in unstable air and −1 in stable air (Priestley and Hill, 1985). With this high correlation, the humidity contribution will appear either as an increase or decrease in the amplitude of the temperature fluctuations, depending on stability. Recognizing that the humidity contribution to uncertainty in T_v is a factor of 5 smaller than for T, we write the expression for the standard deviation of temperature as

$$\sigma_{T_s} \simeq [\sigma_T^2 + 0.2\overline{e'T'}]^{1/2} . \tag{6}$$

Following micrometeorological convention, we use primes to denote deviations from the mean and overbars to denote time averaging. The expression in (6) suggests that $\sigma_{T_s} > \sigma_T$ in unstable air and $< \sigma_T$ in stable air, a test that is both unambiguous and easy to perform.

The comparable expression for the sonic temperature flux is

$$\overline{w'T_s'} \simeq \overline{w'T'} + 0.1\,\overline{w'e'} . \tag{7}$$

The humidity flux term is usually positive (except rarely when the surface is very dry), which implies $\overline{w'T_s'} > \overline{w'T'}$ much of the time. There will be no switch in sign of the humidity effect with stability as in σ_{T_s}.

The magnitude of the deviations can be predicted from the findings of Schotanus *et al.* (1983), who report departures on the order of 5% from σ_T and 10% from $\overline{w'T'}$. (The corresponding departures from σ_{T_v} and $\overline{w'T_v'}$ should be 1% and 2%, respectively, well within the experimental error in most field observations.)

4. Test Results

The scatter diagrams in Figures 1 and 2 summarize our findings from Test No. 1 (Kaimal *et al.*, 1990) conducted on 9 August 1988, 1730–2050 MST. In this test, the ATI probe (designated *K*1 in the figures) is compared with the standard BAO sonic probe with its fine-wire platinum temperature probe mounted close to its vertical path. The two sonic anemometer probes were separated 1 m apart laterally with respect to the wind direction. This was a windy (5–9 m s^{-1}), near-neutral period, a worst-case scenario for the sonic thermometer.

In Figure 1 we can see that the V_n^2 correction brings the data points closer to the 1:1 line. The points separate almost perfectly according to stability, with the slightly unstable 10-min periods (the four points on the left, above the 1:1 line) falling on one side of the line and most of the remaining points, representing slightly stable periods, on the other side, very much as we predicted from (6). The V_n^2 error acts in the same direction as humidity, raising σ_{T_s} in unstable air

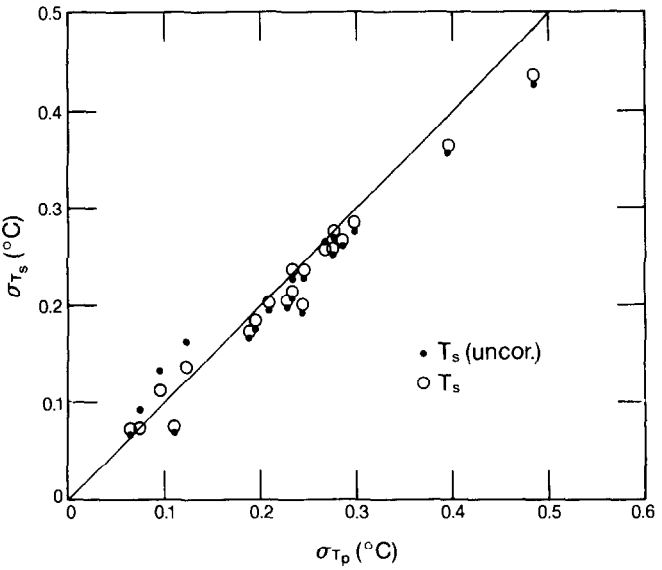

Fig. 1. Ten-minute averaged sonic temperature standard deviations, corrected and uncorrected for velocity contamination, plotted against standard deviations for the platinum wire temperature.

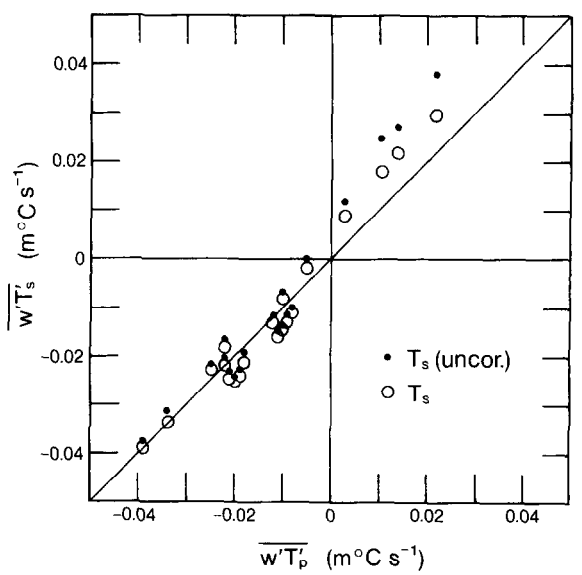

Fig. 2. Ten-minute averaged sonic temperature fluxes, corrected and uncorrected for velocity contamination, plotted against platinum wire temperature fluxes.

(with one exception: very close to neutral) and lowering it in stable air, relative to σ_{T_p}. This follows from the approximate form for $\sigma^2_{T_s}$ in Appendix B:

$$\sigma_{T_s}(\text{uncor}) \approx [\sigma^2_{T_s} - 4\bar{u}\overline{u'T_s'}/403]^{1/2}, \tag{8}$$

where $\bar{u}$ and u' are the mean and fluctuating components of the streamwise wind

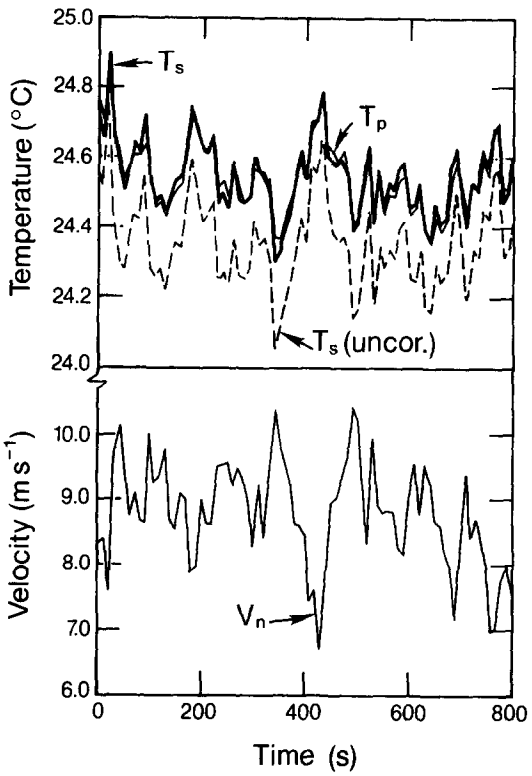

Fig. 3. Ten-second averaged time series of corrected sonic temperature (T_s), uncorrected sonic temperature (T_s uncor), platinum wire temperature (T_p), and crosswind (V_n) showing the effect of the velocity correction during a windy near-neutral period starting at 1730 MST on 9 August 1988.

component. $\overline{u'T'}$ is negative in unstable air and positive in stable air, and its removal brings the measured standard deviation closer to σ_{T_p} (within 5%) in either case.

The V_n^2 error in the temperature flux also raises the flux estimate in unstable air and lowers it in stable air (Figure 2). This too follows from the expression for $\overline{w'T_s'}$ in Appendix B:

$$\overline{w'T_s'}(\text{uncor}) \approx \overline{w'T_s'} - 2\bar{u}\overline{u'w'}/403\,. \tag{9}$$

Because $\overline{u'w'}$ is negative near the ground, the error term will always be positive. According to (7), the corrected fluxes should all fall above the 1:1 line but several of the stable cases do not. The contribution from $\overline{w'e'}$ seems to be lost in the larger scatter of the data points.

As further argument for removing V_n^2, we present in Figure 3 an 800-s segment of 10-s averaged data points from the beginning of Test No. 1 when the wind speeds were the highest (~9 m s^{-1}). The effect of the V_n^2 correction is to raise the mean level of T_s but decrease its amplitude (because of the prevailing negative correlation between V_n and T_s), bringing the fluctuation levels closer to that of

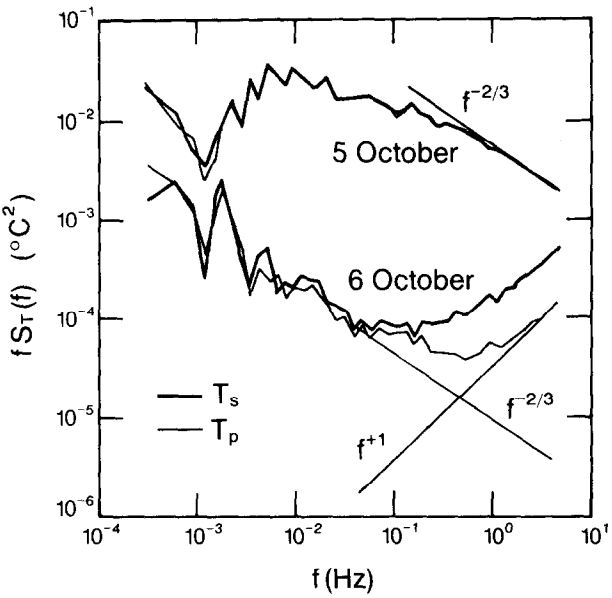

Fig. 4. Spectra from 1-h runs on 5 October 1988 (unstable) and 6 October 1988 (stable) when winds ranged from light to very light.

T_p. Peak amplitudes in T_s are slightly larger than in T_p, as would be expected in unstable air. Note that the placement of T_p in Figure 3 is arbitrary since T_p was not calibrated for absolute accuracy.

The unstable period in Test No. 2 (5 October 1988, 1220–1320 MST) yielded power spectra of T_s and T_p that agreed remarkably well through the whole frequency range (Figure 4), confirming our confidence in the scaling parameters derived in (4). Wind speeds were low (2.5–4 m s^{-1} at 22 m height) during this run.

The stable period in Test No. 2 (6 October 1988, 0220–0320 MST) brings less welcome news in the form of a high noise threshold for T_s (Figure 4). The f^{+1} rise observed at higher frequencies is usually attributed to white noise. Close examination of the T_s and T_p signals reveals random back-and-forth shifts corresponding to the bit resolution in their respective digital outputs. Only the shifts in T_s are larger (~0.06°C) compared to T_p (0.04°C). The rise in the spectrum becomes apparent when spectral levels drop below 10^{-4} °C^2. Wind speeds were very low (1.5–2.5 m s^{-1}) for the duration of this run.

5. Conclusions

Fluctuations in the sonic temperature, corrected for crosswind contamination, should closely approximate fluctuations in the virtual temperature of air. In applications where the virtual temperature is needed to include the buoyant contribution from water vapor, the sonic temperature could be used with negligible loss of accuracy without concurrent measurement of humidity fluctuations to convert

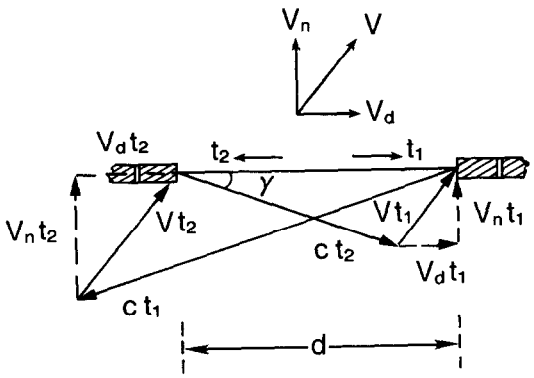

Fig. A-1. Sound ray vectors along a sonic anemometer-thermometer axis.

temperatures to virtual temperatures. Our preliminary tests indicate that the sonic temperature standard deviations behave as predicted in unstable and stable air. The main limitation in sonic thermometers is a noise threshold higher than what we have come to expect in platinum wire thermometers. We need to perform further tests to establish whether T_s, properly corrected for humidity, matches T exactly in its details, and if so, under what conditions $T_s - T$ can be relied on to provide an accurate measure of humidity.

Acknowledgements

We wish to acknowledge the help and cooperation extended to us by the staff of ATI during our tests on their sonic anemometer-thermometer and for extensive discussions on the instrument's precision and resolution. We are grateful to Norbert Szczepczynski and David Gregg for expertly carrying out the tests, to Amy Wyngaard for the computer analysis and plotting of the data, and to John Wyngaard and Christopher Fairall for many helpful discussions and comments on the manuscript. We thank our anonymous reviewer for pointing out an error in the original manuscript.

Appendix A: Principle of Sonic Thermometry

In most sonic anemometer-thermometers, the temperature signal is derived from transit time measurements made along its vertical path because it offers unobstructed azimuth coverage. If t_1 and t_2 are the transit times for sound pulses traveling in opposite directions along path length d (Figure A-1), V_d the wind velocity component along d, and V_n the component normal to it, we have

$$t_1 = d/(c \cos \gamma - V_d)\,, \tag{A-1}$$

$$t_2 = d/(c\cos\gamma + V_d)\,, \tag{A-2}$$

where $\gamma = \sin^{-1}(V_n/c)$. From (A-1) and (A-2), we have

$$(1/t_1) + (1/t_2) = (2/d)c\cos\gamma$$
$$= (2/d)(c^2 - V_n^2)^{1/2}\,. \tag{A-3}$$

Substituting for c^2 from (1) and (3), we have

$$T_s = (d^2/1612)[(1/t_1) + (1/t_2)]^2 + V_n^2/403\,, \tag{A-4}$$

where T_s is the sonic temperature that very closely approximates the virtual temperature of air.

Appendix B: Velocity Error Approximations

We can rewrite (4) in the form

$$T_s(\text{uncor}) = T_s - V_n^2/403\,, \tag{B-1}$$

where $T_s(\text{uncor})$ represents the first estimate of temperature from the transit times t_1 and t_2. Equation (B-1) may be expressed in terms of the streamwise velocity component u and the lateral component v as

$$T_s(\text{uncor}) = T_s - (u^2 + v^2)/403\,. \tag{B-2}$$

Separating the terms into their mean and fluctuating parts and neglecting higher order terms we have

$$T_s'(\text{uncor}) = T_s' - (2\bar{u}u' + 2\bar{v}v')/403\,. \tag{B-3}$$

Squaring both sides and again neglecting higher-order terms,

$$\sigma_{T_s}^2(\text{uncor}) \approx \sigma_{T_s}^2 - (4\bar{u}\overline{u'T_s'} + 4\bar{v}\overline{v'T_s'})/403$$
$$\approx \sigma_{T_s}^2 - 4\bar{u}\overline{u'T_s'}/403\,, \tag{B-4}$$

since $\overline{v'T_s'} \approx 0$ in steady flow over level ground. It also follows that

$$\overline{w'T_s'}(\text{uncor}) = \overline{w'T_s'} - (2\bar{u}\overline{u'w'} + 2\bar{v}\overline{v'w'})/403$$
$$\approx \overline{w'T_s'} - 2\bar{u}\overline{u'w'}/403\,, \tag{B-5}$$

since $\overline{v'w'}$ also vanishes under the same conditions.

References

Hanafusa, T., Fujitani, T., Kobori, Y., and Mitsuta, Y.: 1982, 'A New Type Sonic Anemometer-Thermometer for Field Operation', *Pap. Meteorol. Geophys.* **33**, 1–19.

Kaimal, J. C.: 1969, 'Measurement of Momentum and Heat Flux Variations in the Surface Boundary Layer', *Radio Sci.* **4**, 1147–1153.

Kaimal, J. C. and Businger, J. A.: 1963, 'A Continuous Wave Sonic Anemometer-Thermometer', *J. Appl. Meteorol.* **2**, 156–164.

Kaimal, J. C. and Gaynor, J. E.: 1983, 'The Boulder Atmospheric Observatory', *J. Appl. Meteorol.* **22**, 863–880.

Kaimal, J. C., Gaynor, J. E., Zimmerman, H. A., and Zimmerman, G. A.: 1990, 'Minimizing Flow Distortion Errors in a Sonic Anemometer', *Boundary-Layer Meteorol.* **53**, 103–115.

May, P. T., Strauch, R. G., Moran, K. P., and Ecklund, W. L.: 1990, 'Temperature Sounding by RASS with Wind Profiler Radars', *IEEE Trans. Geosci. Remote Sens.* **28**, 19–28.

Miller, D. C.: 1937, *Sound Waves – Their Shape and Speed*, The Macmillan Co., New York, 164 pp.

Mitsuta, Y.: 1966, 'Sonic Anemometer-Thermometer for General Use', *J. Meteorol. Soc. Japan* **44**, 12–24.

Mitsuta, Y.: 1974, 'Sonic Anemometer-Thermometer for Atmospheric Turbulence Measurements', in R. B. Dowdell (ed.), *Flow – Its Measurement and Control in Science and Industry*, *Vol.* 1, Instrument Society of America, 341–347.

Priestley, J. T. and Hill, R. J.: 1985, 'Measuring High-Frequency Humidity, Temperature and Radio Refractive Index in the Surface Layer', *J. Atmos. Oceanic Technol.* **2**, 233–251.

Schmitt, K. F., Friehe, C. A., and Gibson, C. H.: 1978, 'Humidity Sensitivity of Atmospheric Temperature Sensors by Salt Contamination', *J. Phys. Oceanogr.* **8**, 151–161.

Schotanus, P., Nieuwstadt, F. T. M., and DeBruin, H. A. R.: 1983, 'Temperature Measurement with a Sonic Anemometer and its Application to Heat and Moisture Fluctuations', *Boundary-Layer Meteorol.* **26**, 81–93.

Suomi, V. E.: 1957, 'Energy Budget Studies and Development of the Sonic Anemometer for Spectrum Analysis', AFCRC Tech. Report 56-274, University of Wisconsin, Dept. of Meteorology, 91 pp.